Quantum Phase Diagram and Spontaneously Emergent Topological Chiral Superconductivity in Doped Triangular-Lattice Mott Insulators

Yixuan Huang[1,2,3] Shou-Shu Gong[4,*] and D. N. Sheng[1,†]

[1]*Department of Physics and Astronomy, California State University, Northridge, California 91330, USA*
[2]*Theoretical Division, Los Alamos National Laboratory, Los Alamos, New Mexico 87545, USA*
[3]*Center for Integrated Nanotechnologies, Los Alamos National Laboratory, Los Alamos, New Mexico 87545, USA*
[4]*Department of Physics, Beihang University, Beijing 100191, China*

The topological superconducting state is a highly sought-after quantum state hosting topological order and Majorana excitations. In this Letter, we explore the mechanism to realize the topological superconductivity (TSC) in the doped Mott insulators with time-reversal symmetry (TRS). Through large-scale density matrix renormalization group study of an extended triangular-lattice t-J model on the six- and eight-leg cylinders, we identify a $d + id$-wave chiral TSC with spontaneous TRS breaking, which is characterized by a Chern number $C = 2$ and quasi-long-range superconducting order. We map out the quantum phase diagram with by tuning the next-nearest-neighbor (NNN) electron hopping and spin interaction. In the weaker NNN-coupling regime, we identify a pseudogaplike phase with a charge stripe order coexisting with fluctuating superconductivity, which can be tuned into d-wave superconductivity by increasing the doping level and system width. The TSC emerges in the intermediate-coupling regime, which has a transition to a d-wave superconducting phase with larger NNN couplings. The emergence of the TSC is driven by geometrical frustrations and hole dynamics which suppress spin correlation and charge order, leading to a topological quantum phase transition.

Introduction.—The fractional quantum Hall states discovered in two-dimensional (2D) electron systems under external magnetic fields [1,2] are remarkable states of matter demonstrating topological orders and fractionalized excitations [3–5]. In 2D Mott insulators, geometrical frustration and quantum fluctuations can suppress magnetic order and lead to a topologically ordered quantum spin liquid (QSL) [6–8]. Tuning Mott insulators with doping, more exotic phases including unconventional superconductivity (SC) and non-Fermi liquid emerge [9–17], which are central topics in condensed matter physics. Interestingly, there is a class of time-reversal-symmetry (TRS) breaking QSL named the chiral spin liquid (CSL), which was first proposed by Kalmeyer and Laughlin (KL) as the analog of the fractional quantum Hall state [18]. Remarkably, doping a CSL may lead to $d + id$-wave topological superconductivity (TSC) through the condensation of paired fractional quasiparticles [19–21].

Recently, the KL-CSL has been theoretically discovered in the kagome spin systems with competing interactions [22–25], and near the metal-insulator transition in the triangular Hubbard model [26–28] through spontaneous TRS breaking. Numerical studies on the doped CSL in these systems [25,26] have uncovered either a Wigner crystal solid or a nonsuperconducting chiral metal [29–31], which challenge the original proposal of realizing a TSC [19–21] and demonstrate the richness of doped frustrated systems [32–48]. A breakthrough comes from density

matrix renormalization group (DMRG) studies, which have identified a $d + id$-wave TSC by doping either a CSL [49,50] or a weak Mott insulator [50] in the triangular-lattice t-J model with three-spin chiral coupling J_χ breaking TRS explicitly. Despite the exciting progress, the mechanism of realizing TSC in the systems with TRS remains an outstanding issue, which demands unbiased numerical study beyond mean-field and variational treatments [33–40,51–54]. Focusing on TRS triangular systems, previous DMRG study of the doped J_1-J_2 QSL identified a d-wave SC [55] while the rich interplay among conventional orders, hole dynamics, and spin fluctuations has not been extensively explored in such systems, which may provide a new mechanism to realize TSC through spontaneous TRS breaking.

Experimentally, triangular-lattice compounds are among the most promising candidates for hosting topological states, including the QSL candidates of weak Mott insulators [56–58], the $d + id$-wave TSC candidates $Na_xCoO_2 \cdot yH2O$ [59–61] and $Sn/Si(111)$ systems [62], and the twisted transition metal dichalcogenides (TMD) moiré systems which can simulate the Hubbard and related t-J model [63,64]. The correlated insulators and possible SC states discovered in these systems [65–67] also call for theoretical understanding of the rich interplay among the experimentally tunable parameters such as electronic hopping and interaction.

In this Letter, we study the quantum phases in the extended triangular t-J model using DMRG simulations. By tuning the ratios of the next-nearest-neighbor (NNN) to nearest-neighbor (NN) hopping t_2/t_1 and spin interaction J_2/J_1, we find a pseudogaplike phase with charge density wave (CDW) order at small NNN couplings, which coexists with both the strong spin density wave fluctuation (SDWF) and fluctuating superconductivity (FSC) showing a tendency to develop into a d-wave SC on a wider nine-leg cylinder. With growing t_2/t_1 or (and) J_2/J_1, we identify a phase transition to an emergent $d + id$-wave TSC [19–21,40,68,69] characterized by a topological Chern number $C = 2$, through spontaneous TRS breaking. The SC pairing correlations show algebraic decay with the power exponent $K_{SC} \approx 1.0$ dominating other spin and charge correlations, which are the quasi-1D descendent states of 2D topological superconductors. For even larger NNN couplings, a nematic d-wave SC phase emerges with anisotropic pairing correlations breaking rotational symmetry, which belongs to the same SC phase found in the doped J_1-J_2 QSL [55]. Our results establish a new route to the TSC by doping either a magnetic Mott insulator or a QSL with TRS, in which hole dynamics and geometrical frustrations play essential roles to suppress magnetic correlations and induce the TSC.

Theoretical model and method.—We study the following extended t-J model on the triangular lattice:

$$H = \sum_{\{ij\},\sigma} - t_{ij}(\hat{c}_{i,\sigma}^\dagger \hat{c}_{j,\sigma} + \text{H.c.}) + \sum_{\{ij\}} J_{ij}\left(\hat{\boldsymbol{S}}_i \cdot \hat{\boldsymbol{S}}_j - \frac{1}{4}\hat{n}_i\hat{n}_j\right),$$

where $\hat{c}_{i,\sigma}^\dagger$ ($\hat{c}_{i,\sigma}$) creates (annihilates) an electron on site i with spin $\sigma = \pm 1/2$, $\hat{\boldsymbol{S}}_i$ is the spin-1/2 operator, $\hat{n}_i = \sum_\sigma \hat{c}_{i,\sigma}^\dagger \hat{c}_{i,\sigma}$ is the electron number operator. We tune the ratios of neighboring couplings t_2/t_1 and J_2/J_1 to explore their interplay in driving different phases in the system. We set $J_1 = 1$ as the energy unit and $t_1/J_1 = 3$ to mimic a strong Hubbard interaction $U/t = 12$.

We perform large scale DMRG simulations with charge $U(1)$ and spin $SU(2)$ symmetries [70–72] on a cylinder system, which has an open boundary in the e_a or x direction and periodic boundary conditions in the e_b or y direction [Fig. 1(a)]. The number of sites along the x (y) direction is denoted as L_x (L_y) and the total number of sites is $N = L_x \times L_y$. The electron number N_e is related to hole doping level δ as $N_e/N = 1 - \delta$. We focus on the results on the $L_y = 6$ systems, which are supplemented with the studies on wider $L_y = 8$, 9 cylinders [73]. We keep up to $M = 20\,000$ $SU(2)$ multiplets [equivalent to about $60\,000$ $U(1)$ states] to obtain accurate results with the truncation error $\epsilon \lesssim 2 \times 10^{-5}$; see more details in Sec. I. of the Supplemental Material (SM) [74].

Phase diagram and Chern number characterization.—We map out the phase diagram for $\delta = 1/12$ based on the results of the Chern number [50] and pairing correlation. As
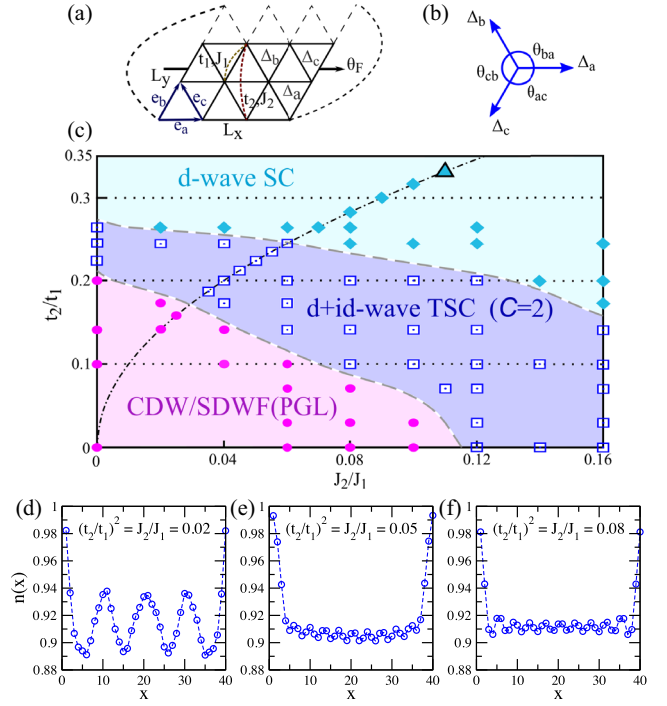

FIG. 1. Global quantum phase diagram. (a) Schematic figure of the triangular t-J model with the NN and NNN hoppings t_1, t_2 and spin interactions J_1, J_2. θ_F is the magnetic flux threading in the cylinder. $\Delta_{a,b,c}$ define the pairing order parameters of the NN bonds along the $e_{a,b,c}$ directions. (b) The relative phases between $\Delta_\alpha = |\Delta_\alpha|e^{i\theta_\alpha}$ ($\alpha = a$, b, c), defined as $\theta_{\alpha\beta} = \theta_\alpha - \theta_\beta$. (c) The quantum phase diagram obtained on the $L_y = 6$ cylinder with doping level $\delta = 1/12$. We identify a pseudogaplike (PGL) phase with CDW/SDWF, a $d + id$-wave TSC phase, and a d-wave SC phase. The dotted dashed line denotes $J_2/J_1 = (t_2/t_1)^2$. The symbols mark the studied parameters, and the cyan triangle marks the studied parameter in Ref. [55]. (d)–(f) The charge density profile in the three phases. $n(x)$ is the charge density per site in each column x, obtained on the 40×6 cylinder with $M = 12\,000$.

shown in the phase diagram [Fig. 1(c)], in the smaller J_2 and t_2 regime we identify a pseudogaplike phase [75,76] with dominant CDW order and short-range d-wave SC fluctuation. The TSC emerges in the intermediate coupling regime while the previously identified d-wave SC phase [55] appears at the larger NNN couplings.

To identify the topological nature of the phases, we perform the inserting flux simulation [23,50] using the infinite DMRG [77] with increasing the flux adiabatically with $\theta_F \to \theta_F + \Delta\theta_F$ and $\Delta\theta_F = 2\pi/16$. We measure the accumulated spin $Q_s = n_\uparrow - n_\downarrow$ at left edge for each θ_F (n_σ is the total charge with spin σ near the edge [50]). For a range of intermediate NNN couplings, nonzero pumped spin ΔQ_s is obtained, which increases almost linearly with θ_F [Fig. 2(a)], indicating the uniform Berry curvature [78]. By threading a flux quantum ($\theta_F = 0 \to 2\pi$), the Chern number $C = \Delta Q_s \approx 2.0$ characterizes a robust TRS-breaking topological state. The energy per site E_0 varies
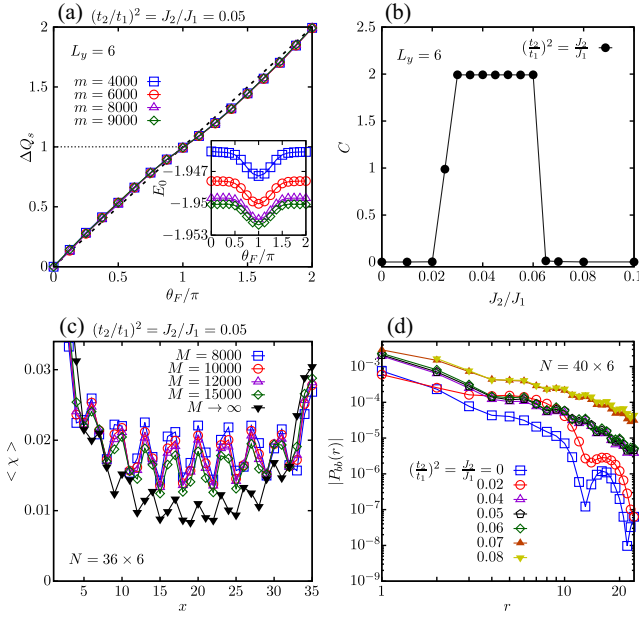
FIG. 2. Identifying the TSC phase and phase transitions along $(t_2/t_1)^2 = J_2/J_1$. (a) Spin pumping simulation by adiabatically inserting flux θ_F for $J_2/J_1 = 0.05$. m is the $U(1)$ bond dimension. By inserting a flux quantum, we obtain the Chern number $C = \Delta Q_s \approx 2$ with an error smaller than ± 0.03. The inset shows the flux dependence of ground-state energy per site E_0. (b) Coupling dependence of the obtained Chern number with $m = 8000$. (c) Spin chiral order $\langle \chi \rangle = \langle \hat{S}_i \cdot (\hat{S}_j \times \hat{S}_k) \rangle$ of the triangles in each column versus the column position x for $J_2/J_1 = 0.05$. M is the $SU(2)$ bond dimension. (d) Double-logarithmic plot of the pairing correlation $|P_{bb}(r)|$ obtained with $M = 12\,000$.

smoothly with θ_F [the inset of Fig. 2(a)], indicating a gapped spectrum flow and robust topological quantization [79]. Here $C = 2$ identifies the number of chiral Majorana edge modes [68,69]. In Fig. 2(b), we show the obtained Chern number along $(t_2/t_1)^2 = J_2/J_1$, where the quantized $C = 2$ clearly distinguishes the TSC from the topologically trivial phases with $C = 0$ nearby (see more results in SM Sec. II. [74]). We further show the chiral order $\langle \chi \rangle = \langle \hat{S}_i \cdot (\hat{S}_j \times \hat{S}_k) \rangle$ (the sites i, j, k belong to the smallest triangle) along the x direction [Fig. 2(c)]. The chiral orders after bond-dimension scaling to $M \to \infty$ limit remain finite, supporting the spontaneous TRS breaking in the TSC.

Next, we show the evolution of the dominant spin-singlet pairing correlations $P_{\alpha\beta}(\mathbf{r}) = \langle \hat{\Delta}_\alpha^\dagger(\mathbf{r}_0)\hat{\Delta}_\beta(\mathbf{r}_0 + \mathbf{r}) \rangle$ where the pairing order is defined as $\hat{\Delta}_\alpha(\mathbf{r}) = (\hat{c}_{\mathbf{r}\uparrow}\hat{c}_{\mathbf{r}+e_\alpha\downarrow} - \hat{c}_{\mathbf{r}\downarrow}\hat{c}_{\mathbf{r}+e_\alpha\uparrow})/\sqrt{2}$ ($\alpha = a$, b, c). The pairing correlation $|P_{bb}(r)|$ decays very fast for $t_2 = J_2 = 0$ and is enhanced at short distance for $(t_2/t_1)^2 = J_2/J_1 = 0.02$ inside the CDW + SDWF phase [Fig. 2(d)]. With larger NNN couplings in the TSC and d-wave SC phases, pairing correlations are strongly enhanced at all distances.

Spin structure factor and charge occupation.—Now we discuss the spin correlation and charge occupation.
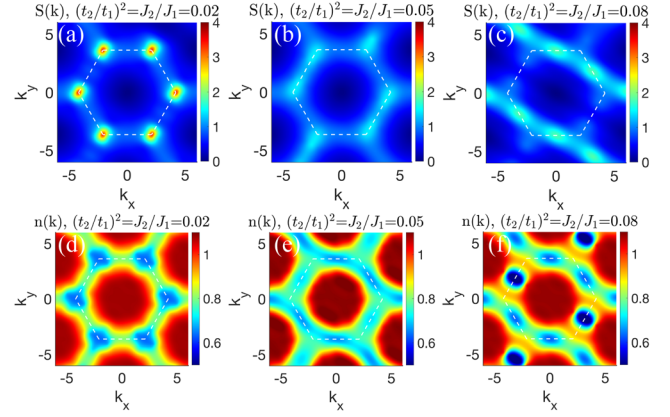

FIG. 3. Spin structure factor $S(\mathbf{k})$ and electron density in momentum space $n(\mathbf{k})$ in the three phases. The results are obtained using the middle $N_m = 24 \times 6$ sites of a long cylinder, which are calculated with $M = 12\,000$ and well converged. The dashed hexagon denotes the Brillouin zone. (a) and (d) belong to the CDW + SDWF phase, (b) and (e) belong to the TSC phase, (c) and (f) belong to the d-wave SC phase.

In the CDW + SDWF phase, the spin structure factor $S(\mathbf{k}) = (1/N_m)\sum_{i,j}\langle \hat{S}_i \cdot \hat{S}_j \rangle e^{i\mathbf{k}\cdot(\mathbf{r}_i - \mathbf{r}_j)}$ has prominent peaks at the $\mathbf{K}$ points representing strong $120°$ spin fluctuation [Fig. 3(a)]. In the TSC, the $\mathbf{K}$ point peaks are significantly suppressed and dispersed along one of the edges of Brillouin zone [see Fig. 3(b) and SM Sec. III. [74]], consistent with the emergence of the CSL in spin background. In the d-wave SC phase, weak peaks emerge at two $\mathbf{M}$ points [Fig. 3(c)], indicating nematic spin fluctuation. Furthermore, we investigate the electron occupation number in the momentum space $n(\mathbf{k}) = (1/N_m)\sum_{i,j,\sigma}\langle \hat{c}_{i,\sigma}^\dagger \hat{c}_{j,\sigma} \rangle e^{i\mathbf{k}\cdot(\mathbf{r}_i - \mathbf{r}_j)}$ and find that from the CDW + SDWF phase to the TSC, the hole pockets at the $\mathbf{K}$ points disperse along the edge of the Brillouin zone, while in the d-wave SC phase the hole pockets concentrate at two $\mathbf{M}$ points [Figs. 3(d)–3(f) and SM Sec. VII. [74]]. In real space, the charge density profile in the CDW + SDWF phase shows a strong stripe pattern with the wavelength $\lambda \approx 10$ while in the SC phases, the CDW becomes much weaker with $\lambda \approx 4$ [Figs. 1(d)–1(f)].

Fluctuating superconductivity in the CDW + SDWF *phase.*—To reveal the nature of the CDW + SDWF phase, we focus on the correlation functions. At $t_2 = J_2 = 0$, the extrapolated spin correlations $S(\mathbf{r}) = \langle \hat{S}_{\mathbf{r}_0} \cdot \hat{S}_{\mathbf{r}_0 + \mathbf{r}} \rangle$ decay exponentially with a large correlation length $\xi_S \approx 9.2$ (6.9) on the $L_y = 6$ (9) system [Fig. 4(a)], confirming the absence of magnetic order and short-range SDWF. We further compare $S(r)$ with single-particle correlation $G(\mathbf{r}) = \sum_\sigma \langle \hat{c}_{\mathbf{r}_0,\sigma}^\dagger \hat{c}_{\mathbf{r}_0 + \mathbf{r},\sigma} \rangle$, density correlation $D(\mathbf{r}) = \langle \hat{n}_{\mathbf{r}_0}\hat{n}_{\mathbf{r}_0 + \mathbf{r}} \rangle - \langle \hat{n}_{\mathbf{r}_0}\rangle\langle \hat{n}_{\mathbf{r}_0 + \mathbf{r}}\rangle$, and pairing correlation $|P_{bb}(r)|$ using the extrapolated $M \to \infty$ data (rescaled with doping ratio for direct comparison) as shown in Fig. 4(b). While the spin correlation is relatively strong, single-particle $|G(r)|$ decays exponentially with a short correlation length $\xi_G \approx 3.7$.
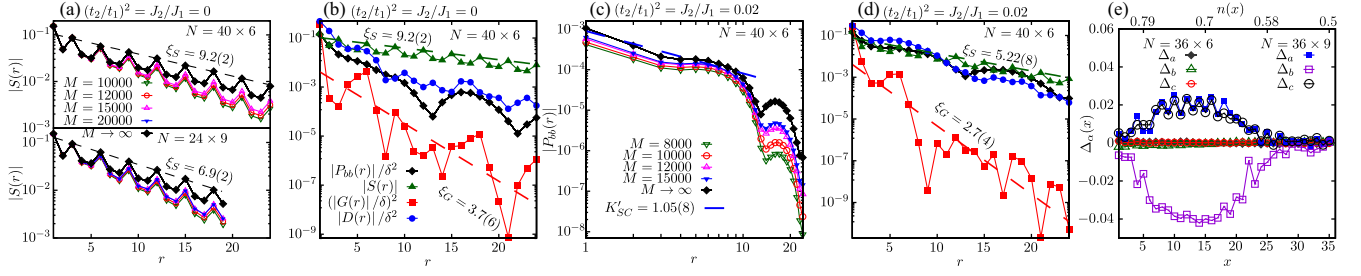
FIG. 4.   Correlation functions and SC orders in the CDW + SDWF phase with extrapolated $M \to \infty$ data for (a)–(d). (a) Logarithmic-linear plots of the spin correlations on the 40×6 and 24×9 cylinders, with the correlation length $\xi_S = 9.2(2)$ $(6.9(2))$ for $L_y = 6$ (9). The number in the bracket gives the standard deviation from linear fitting. (b) Comparing correlations which are rescaled with doping ratio for a direct comparison. The fittings give $\xi_S = 9.2(2)$ and $\xi_G = 3.7(6)$. (c) Double-logarithmic plot of pairing correlation $|P_{bb}(r)|$. The extrapolated results with $r \leq 10$ can be fitted algebraically with $K'_{SC} = 1.05(8)$. (d) Comparing correlations where the fittings give $\xi_S = 5.22(8)$ and $\xi_G = 2.7(4)$. We choose the reference site at $x_0 = L_x/4$ for demonstrating correlations. (e) Different SC orders Δ_α versus each column x for a system in a grand canonical ensemble with $M = 8000$ and the averaged electron density $n(x)$. The coupling parameters are the same as (d). A varying chemical potential $\mu_i = \mu(x) = \mu_0 + x/L_x[a + b(x/L_x)]$ is used to adjust the range of $n(x)$.

Although the pairing correlation also decays fast, it is much stronger compared to the two single-particle correlator $|G^2(r)|$, indicating the more suppressed single-particle channel.

At $(t_2/t_1)^2 = J_2/J_1 = 0.02$, $|P_{bb}(r)|$ is enhanced and decays algebraically with an exponent $K'_{SC} \approx 1.05$ within short distance, which indicates a strong local pairing order [Fig. 4(c) and Fig. 2(d)] representing the FSC. Remarkably, the difference between $|P_{bb}(r)|$ and $|G^2(r)|$ dramatically increases with $|P_{bb}(r)|$ larger than $|G^2(r)|$ by around 4 orders of magnitude at large distances [Fig. 4(d)], unveiling the "pseudogap" behavior. To further explore the FSC, we compute the SC order in the grand canonical ensemble with varying chemical potential $H \to H - \sum_i \mu_i n_i$ following the method in Ref. [80] (see SM Sec. VIII. [74]). As shown in Fig. 4(e), a finite d-wave SC order develops with increased $L_y = 9$ and the doping level over 20%.

$d + id$-wave TSC phase.—Next we turn to the characterization of the TSC phase. By bond-dimension extrapolation, we identify the algebraic decay of the pairing correlation. For $(t_1/t_2)^2 = J_1/J_2 = 0.05$ and $L_y = 6$, we find $|P_{bb}(r)| \sim r^{-K_{SC}}$ with $K_{SC} \approx 1.03$ [Fig. 5(a)], indicating a divergent SC susceptibility in the zero-temperature limit [81]. Similar results are also obtained on the wider $L_y = 8$ system (see SM Sec. V.A. [74]), supporting the robust TSC.

To identify the pairing symmetry, we rewrite $\Delta_\alpha(\mathbf{r}) = |\Delta_\alpha(\mathbf{r})|e^{i\theta_\alpha(\mathbf{r})}$ and $P_{\alpha\beta}(\mathbf{r}) = |P_{\alpha\beta}(\mathbf{r})|e^{i\phi_{\alpha\beta}(\mathbf{r})}$ with the relative phases $\phi_{\alpha\beta}(\mathbf{r}) = \theta_\beta(\mathbf{r}_0 + \mathbf{r}) - \theta_\alpha(\mathbf{r}_0)$. Thus, $\theta_{\alpha\beta}(\mathbf{r}) \equiv \theta_\alpha(\mathbf{r}) - \theta_\beta(\mathbf{r}) = \phi_{\alpha\alpha}(\mathbf{r}) - \phi_{\alpha\beta}(\mathbf{r})$ [see Fig. 1(b)]. As shown in Fig. 5(b), $\phi_{\alpha\beta}(r)$ are nearly uniform in real space and are obtained as $[\phi_{bb}, \phi_{bc}, \phi_{ba}] = [0.000(4), 0.61(2)\pi, -0.61(2)\pi] \approx [0, \frac{2}{3}\pi, -\frac{2}{3}\pi]$ for $L_y = 6$, which give $\theta_{ba} = \theta_{ac} = \theta_{cb} \approx 2\pi/3$ characterizing an isotropic $d + id$-wave pairing symmetry, while $\theta_{ba} = \theta_{cb} = \pi$ is observed in the d-wave SC phase. We also confirm this robust pairing symmetry on the wider $N = 36 \times 8$ system [see Fig. 5(b) and SM Sec. V.A. [74]], providing compelling evidence for
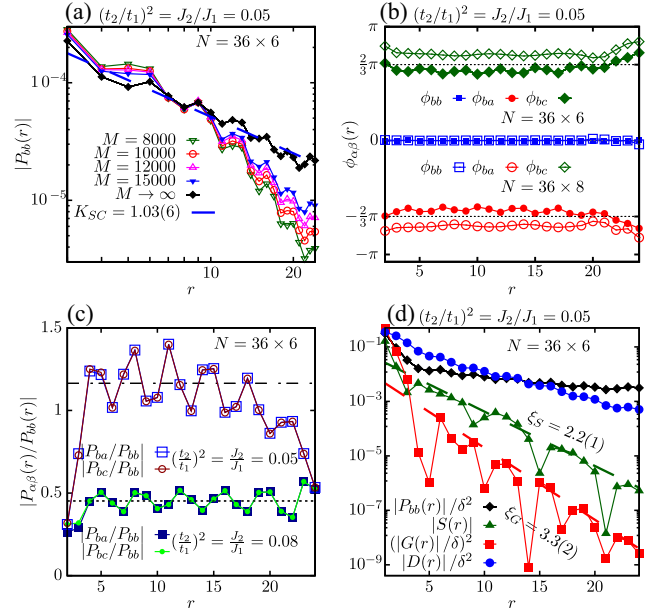

FIG. 5.   Correlation functions for $(t_2/t_1)^2 = J_2/J_1 = 0.05$ in the TSC phase using the extrapolated data. (a) Double-logarithmic plot of the pairing correlations $|P_{bb}(r)|$ obtained by keeping different $SU(2)$ bond dimensions. The extrapolated correlations decay algebraically with $K_{SC} = 1.03(6)$. (b) $d + id$-wave pairing symmetry identified by the phase differences of pairing correlations on the $L_y = 6$ (8) cylinder using bond dimensions $M = 15\,000$ $(20\,000)$. (c) The ratios of the magnitudes of the pairing correlations at different bonds. The dashed dotted line indicates the averaged ratio of 1.2(1) for the TSC phase. The dotted line indicates the averaged ratio of 0.45(5) for the d-wave SC phase. We choose $r \leq L_x/2$ to calculate the averages to minimize the boundary effect. (d) Comparing the correlations which are rescaled with the doping ratio. The fittings give $\xi_S = 2.2(1)$ and $\xi_G = 3.3(2)$. We choose $x_0 = L_x/4$ and fit the data to the distance $r = L_x/2$ to avoid a boundary effect.

the emergent TSC through spontaneous TRS breaking. Furthermore, as shown in Fig. 5(c), we find that $|P_{ba}(r)/P_{bb}(r)|$ and $|P_{bc}(r)/P_{bb}(r)|$ averaged over r are around 1.2 for the near isotropic TSC phase, while they drop to around 0.45 in the nematic d-wave SC phase.

In comparison, both spin and single-particle correlations decay exponentially with small correlation lengths [Fig. 5(d)] while the density correlations seem also to decay algebraically but with a large exponent $K_{CDW} \approx 2.4$, showing that the pairing correlation dominates all other correlations.

Summary and discussion.—Through DMRG simulation on the extended triangular t-J model, we identify a $d + id$-wave TSC through spontaneous TRS breaking, by doping either a magnetic order state or a time-reversal symmetric QSL. The driving mechanism is the balanced spin frustrations and hole dynamics induced by NNN couplings, which suppress magnetic correlations and lead to the TSC for doping level $\delta = 1/12 - 1/8$ (see additional results in SM Sec. V.B. [74]). Physically, frustration to spin background can be built up by NNN coupling J_2, or t_2, or both terms acting jointly. Our findings open a new route for discovering TSC in correlated materials, with the TMD Moiré super-lattices [64–67] being the most promising platform [63].

We also reveal the pseudogaplike physics in the CDW $+$ SDWF phase, which demonstrates a tendency to evolve into d-wave SC by increasing the phase coherence of pairing correlations. Our Letter suggests a new direction for future studies on doped Mott insulators [72,80–89], which may provide insights to the challenging issues related to the normal states of the high-T_c cuprate superconductors [75,76].

The data and simulation code are available from the corresponding author upon reasonable request.

Note added.—Recently, we noticed a related work, Ref. [90], which studies possible superconductivity with different hopping signs.

*shoushu.gong@buaa.edu.cn
†donna.sheng1@csun.edu

[1] D. C. Tsui, H. L. Stormer, and A. C. Gossard, Phys. Rev. Lett. **48**, 1559 (1982).
[2] R. B. Laughlin, Phys. Rev. Lett. **50**, 1395 (1983).
[3] B. I. Halperin, Phys. Rev. Lett. **52**, 1583 (1984).
[4] X.-G. Wen, Int. J. Mod. Phys. B **04**, 239 (1990).
[5] X. G. Wen, Phys. Rev. B **44**, 2664 (1991).
[6] L. Balents, Nature (London) **464**, 199 (2010).
[7] Y. Zhou, K. Kanoda, and T.-K. Ng, Rev. Mod. Phys. **89**, 025003 (2017).
[8] C. Broholm, R. Cava, S. Kivelson, D. Nocera, M. Norman, and T. Senthil, Science **367**, 6475 (2020).
[9] P. W. Anderson, Science **235**, 1196 (1987).
[10] P. A. Lee, N. Nagaosa, and X.-G. Wen, Rev. Mod. Phys. **78**, 17 (2006).
[11] B. Keimer, S. A. Kivelson, M. R. Norman, S. Uchida, and J. Zaanen, Nature (London) **518**, 179 (2015).
[12] C. Proust and L. Taillefer, Annu. Rev. Condens. Matter Phys. **10**, 409 (2019).
[13] X.-G. Wen and P. A. Lee, Phys. Rev. Lett. **76**, 503 (1996).
[14] E. Fradkin, S. A. Kivelson, and J. M. Tranquada, Rev. Mod. Phys. **87**, 457 (2015).
[15] T. Senthil and P. A. Lee, Phys. Rev. B **71**, 174515 (2005).
[16] L. Balents and S. Sachdev, Ann. Phys. (Amsterdam) **322**, 2635 (2007).
[17] S. Sachdev, Phys. Rev. Lett. **105**, 151602 (2010).
[18] V. Kalmeyer and R. B. Laughlin, Phys. Rev. Lett. **59**, 2095 (1987).
[19] R. B. Laughlin, Phys. Rev. Lett. **60**, 2677 (1988).
[20] X. G. Wen, F. Wilczek, and A. Zee, Phys. Rev. B **39**, 11413 (1989).
[21] D.-H. Lee and M. P. A. Fisher, Phys. Rev. Lett. **63**, 903 (1989).
[22] Y.-C. He, D. N. Sheng, and Y. Chen, Phys. Rev. Lett. **112**, 137202 (2014).
[23] S.-S. Gong, W. Zhu, and D. N. Sheng, Sci. Rep. **4**, 6317 (2014).
[24] B. Bauer, L. Cincio, B. P. Keller, M. Dolfi, G. Vidal, S. Trebst, and A. W. W. Ludwig, Nat. Commun. **5**, 5137 (2014).
[25] S.-S. Gong, W. Zhu, L. Balents, and D. N. Sheng, Phys. Rev. B **91**, 075112 (2015).
[26] A. Szasz, J. Motruk, M. P. Zaletel, and J. E. Moore, Phys. Rev. X **10**, 021042 (2020).
[27] B.-B. Chen, Z. Chen, S.-S. Gong, D. Sheng, W. Li, and A. Weichselbaum, Phys. Rev. B **106**, 094420 (2022).
[28] A. Wietek, R. Rossi, F. Šimkovic, M. Klett, P. Hansmann, M. Ferrero, E. M. Stoudenmire, T. Schäfer, and A. Georges, Phys. Rev. X **11**, 041013 (2021).
[29] H.-C. Jiang, T. Devereaux, and S. A. Kivelson, Phys. Rev. Lett. **119**, 067002 (2017).
[30] C. Peng, Y.-F. Jiang, D.-N. Sheng, and H.-C. Jiang, Adv. Quantum Technol. **4**, 2000126 (2021).
[31] Z. Zhu, D. N. Sheng, and A. Vishwanath, Phys. Rev. B **105**, 205110 (2022).
[32] X.-Y. Song, A. Vishwanath, and Y.-H. Zhang, Phys. Rev. B **103**, 165138 (2021).
[33] G. Baskaran, Phys. Rev. Lett. **91**, 097003 (2003).
[34] B. Kumar and B. S. Shastry, Phys. Rev. B **68**, 104508 (2003).
[35] Q.-H. Wang, D.-H. Lee, and P. A. Lee, Phys. Rev. B **69**, 092504 (2004).
[36] T. Watanabe, H. Yokoyama, Y. Tanaka, J.-i. Inoue, and M. Ogata, J. Phys. Soc. Jpn. **73**, 3404 (2004).
[37] B. Braunecker, P. A. Lee, and Z. Wang, Phys. Rev. Lett. **95**, 017004 (2005).

[38] C. Weber, A. Läuchli, F. Mila, and T. Giamarchi, Phys. Rev. B **73**, 014519 (2006).

[39] J. Y. Gan, Y. Chen, and F. C. Zhang, Phys. Rev. B **74**, 094515 (2006).

[40] S. Zhou and Z. Wang, Phys. Rev. Lett. **100**, 217002 (2008).

[41] K. S. Chen, Z. Y. Meng, U. Yu, S. Yang, M. Jarrell, and J. Moreno, Phys. Rev. B **88**, 041103(R) (2013).

[42] O. I. Motrunich and P. A. Lee, Phys. Rev. B **69**, 214516 (2004).

[43] M. L. Kiesel, C. Platt, W. Hanke, and R. Thomale, Phys. Rev. Lett. **111**, 097001 (2013).

[44] D. P. Arovas, E. Berg, S. A. Kivelson, and S. Raghu, Annu. Rev. Condens. Matter Phys. **13**, 239 (2022).

[45] Y. Gannot, Y.-F. Jiang, and S. A. Kivelson, Phys. Rev. B **102**, 115136 (2020).

[46] C. Peng, Y.-F. Jiang, Y. Wang, and H.-C. Jiang, New J. Phys. **23**, 123004 (2021).

[47] A. M. Aghaei, B. Bauer, K. Shtengel, and R. V. Mishmash, arXiv:2009.12435.

[48] Y.-F. Jiang, H. Yao, and F. Yang, Phys. Rev. Lett. **127**, 187003 (2021).

[49] Y.-F. Jiang and H.-C. Jiang, Phys. Rev. Lett. **125**, 157002 (2020).

[50] Y. Huang and D. N. Sheng, Phys. Rev. X **12**, 031009 (2022).

[51] Z.-C. Gu, H.-C. Jiang, D. N. Sheng, H. Yao, L. Balents, and X.-G. Wen, Phys. Rev. B **88**, 155112 (2013).

[52] C. Xu and L. Balents, Phys. Rev. Lett. **121**, 087001 (2018).

[53] B. Zhou and Y.-H. Zhang, arXiv:2209.10023.

[54] M. Bélanger, J. Fournier, and D. Sénéchal, Phys. Rev. B **106**, 235135 (2022).

[55] H.-C. Jiang, npj Quantum Mater. **6**, 1 (2021).

[56] Y. Kurosaki, Y. Shimizu, K. Miyagawa, K. Kanoda, and G. Saito, Phys. Rev. Lett. **95**, 177001 (2005).

[57] T. Itou, A. Oyamada, S. Maegawa, M. Tamura, and R. Kato, J. Phys. Condens. Matter **19**, 145247 (2007).

[58] S. Yamashita, Y. Nakazawa, M. Oguni, Y. Oshima, H. Nojiri, Y. Shimizu, K. Miyagawa, and K. Kanoda, Nat. Phys. **4**, 459 (2008).

[59] K. Takada, H. Sakurai, E. Takayama-Muromachi, F. Izumi, R. A. Dilanian, and T. Sasaki, Nature (London) **422**, 53 (2003).

[60] R. E. Schaak, T. Klimczuk, M. L. Foo, and R. J. Cava, Nature (London) **424**, 527 (2003).

[61] T. Fujimoto, G.-q. Zheng, Y. Kitaoka, R. L. Meng, J. Cmaidalka, and C. W. Chu, Phys. Rev. Lett. **92**, 047004 (2004).

[62] F. Ming, X. Wu, C. Chen, K. Wang, P. Mai, T. Maier, J. Strockoz, J. Venderbos, C. Gonzalez, J. Ortega *et al.*, Nat. Phys. 1 (2023).

[63] F. Wu, T. Lovorn, E. Tutuc, and A. H. MacDonald, Phys. Rev. Lett. **121**, 026402 (2018).

[64] Y. Tang, L. Li, T. Li, Y. Xu, S. Liu, K. Barmak, K. Watanabe, T. Taniguchi, A. H. MacDonald, J. Shan, and K. F. Mak, Nature (London) **579**, 353 (2020).

[65] L. An, X. Cai, D. Pei, M. Huang, Z. Wu, Z. Zhou, J. Lin, Z. Ying, Z. Ye, X. Feng *et al.*, Nanoscale Horiz. **5**, 1309 (2020).

[66] C. Schrade and L. Fu, arXiv:2110.10172.

[67] M. M. Scherer, D. M. Kennes, and L. Classen, npj Quantum Mater. **7**, 100 (2022).

[68] N. Read and D. Green, Phys. Rev. B **61**, 10267 (2000).

[69] T. Senthil, J. B. Marston, and M. P. A. Fisher, Phys. Rev. B **60**, 4245 (1999).

[70] S. R. White, Phys. Rev. Lett. **69**, 2863 (1992).

[71] I. P. McCulloch, J. Stat. Mech. (2007) P10014.

[72] S. Gong, W. Zhu, and D. N. Sheng, Phys. Rev. Lett. **127**, 097003 (2021).

[73] The DMRG simulations on the $L_y = 4$ system have not found the topological superconductivity with spontaneous time-reversal symmetry breaking in the intermediate-coupling regime. Instead, a phase separation between the hole rich region and electron rich region is found due to the relatively small system circumference; see the supplementary information of Ref. [50].

[74] See Supplemental Material at http://link.aps.org/supplemental/10.1103/PhysRevLett.130.136003 for detailed numerical results and discussions.

[75] P. A. Lee, Phys. Rev. X **4**, 031017 (2014).

[76] Z. Dai, T. Senthil, and P. A. Lee, Phys. Rev. B **101**, 064502 (2020).

[77] A. G. Grushin, J. Motruk, M. P. Zaletel, and F. Pollmann, Phys. Rev. B **91**, 035136 (2015).

[78] D. N. Sheng, Z. Y. Weng, L. Sheng, and F. D. M. Haldane, Phys. Rev. Lett. **97**, 036808 (2006).

[79] Because the time-revesal symmetry is breaking spontaneously, we can identify nonzero Chern number $C = \pm 2$ with equal probability in our DMRG simulation with random initial complex wavefunction.

[80] S. Jiang, D. J. Scalapino, and S. R. White, Proc. Natl. Acad. Sci. U.S.A. **118**, e2109978118 (2021).

[81] H.-C. Jiang and S. A. Kivelson, Phys. Rev. Lett. **127**, 097002 (2021).

[82] S. R. White and D. J. Scalapino, Phys. Rev. B **79**, 220504(R) (2009).

[83] P. Corboz, T. M. Rice, and M. Troyer, Phys. Rev. Lett. **113**, 046402 (2014).

[84] B.-X. Zheng, C.-M. Chung, P. Corboz, G. Ehlers, M.-P. Qin, R. M. Noack, H. Shi, S. R. White, S. Zhang, and G. K.-L. Chan, Science **358**, 1155 (2017).

[85] E. W. Huang, C. B. Mendl, S. Liu, S. Johnston, H.-C. Jiang, B. Moritz, and T. P. Devereaux, Science **358**, 1161 (2017).

[86] Y.-F. Jiang, J. Zaanen, T. P. Devereaux, and H.-C. Jiang, Phys. Rev. Res. **2**, 033073 (2020).

[87] M. Qin, C.-M. Chung, H. Shi, E. Vitali, C. Hubig, U. Schollwöck, S. R. White, and S. Zhang (Simons Collaboration on the Many-Electron Problem), Phys. Rev. X **10**, 031016 (2020).

[88] X. Wu, F. Ming, T. S. Smith, G. Liu, F. Ye, K. Wang, S. Johnston, and H. H. Weitering, Phys. Rev. Lett. **125**, 117001 (2020).

[89] J. Yang, L. Liu, J. Mongkolkiattichai, and P. Schauss, PRX Quantum **2**, 020344 (2021).

[90] Z. Zhu and Q. Chen, arXiv:2210.06847.

Correction: The omission of two affiliations for the first author has been set right. This change necessitated renumbering of the second author's affiliation indicator. The omission of a support statement in the Acknowledgments has been fixed.